AAE 91-11

UILUENG 91-0511

TRANSPORT PROCESSES IN BEAMED ENERGY PROPULSION SYSTEMS

Prepared by:

Robert A. Beddini
Mark J. Mueller

Aerothermal Simulations Laboratory
Department of Aeronautical and Astronautical Engineering
University of Illinois at Urbana-Champaign
104 South Mathews Avenue
Urbana, Illinois 61801

Final Technical Report
AFOSR Grant 89-0308
for the period 1-September-1989 – 30-September-1991

Prepared for:

Air Force Office of Scientific Research, AFSC
Attention: Dr. Mitat Birkan / NA
Building 410
Bolling Air Force Base, DC 20332-6448

November, 1991

REPORT DOCUMENTATION PAGE

1. AGENCY USE ONLY (Leave blank)	2. REPORT DATE	3. REPORT TYPE AND DATES COVERED
	November, 1991	Final, 01/09/89 to 30/09/91

4. TITLE AND SUBTITLE
Transport Processes in Beamed Energy Propulsion Systems

5. FUNDING NUMBERS
6-AFOSR 89-0308

6. AUTHOR(S)
Robert A. Beddini and Mark J. Mueller

7. PERFORMING ORGANIZATION NAME(S) AND ADDRESS(ES)
University of Illinois
Grants and Contracts Office
809 S. Wright
105 Davenport House
Champaign, IL 61820

8. PERFORMING ORGANIZATION REPORT NUMBER

9. SPONSORING MONITORING AGENCY NAME(S) AND ADDRESS(ES)
AFOSR INA
Building 410
Bolling AFB, DC 20332-6448

10. SPONSORING MONITORING AGENCY REPORT NUMBER

11. SUPPLEMENTARY NOTES

12a. DISTRIBUTION AVAILABILITY STATEMENT
Approved for public release;
distribution unlimited

12b. DISTRIBUTION CODE

13. ABSTRACT (*Maximum 200 words*)

A model of a microwave-induced plasma propulsion system has been developed in one dimension for a transverse electric mode (TE_{10}) of operation in a rectangular waveguide. Available experimental data are compared to the computational results for the case of a planar propagating plasma wave and, using a TE_{10} mode-shape approximation, for a wave propagating in a waveguide. Temperature profiles, plasma propagation velocities, velocity profiles, and absorbed power histories are obtained for flow of helium from .5 to 1 atmosphere pressure and 500 to 3000 watts input power at a frequency of 2.45 GHz. The computational results show the observed jumping of the plasma towards the microwave source. Peak plasma temperatures range from 8000 to 9000 K over the input power range. For an input power of 1081.7 W the calculated percentage of power absorbed in approximately 70 percent for the planar case and 40 percent for the waveguide case.

Comparisons with experimental data indicate other mechanisms (not involving transient processes), most likely associated with the nonequilibrium behavior of the plasma, are responsible for the disagreement between the model results and the observed plasma propagation velocities.

14. SUBJECT TERMS
propulsion, microwave, discharge, waveguide, plasma

15. NUMBER OF PAGES
58

16. PRICE CODE

17. SECURITY CLASSIFICATION OF REPORT	18. SECURITY CLASSIFICATION OF THIS PAGE	19. SECURITY CLASSIFICATION OF ABSTRACT	20. LIMITATION OF ABSTRACT
Unclassified	Unclassified	Unclassified	UL

AAE 91-11 UILUENG 91-0511

TRANSPORT PROCESSES IN BEAMED ENERGY PROPULSION SYSTEMS

Prepared by:

Robert A. Beddini
Mark J. Mueller

Aerothermal Simulations Laboratory
Department of Aeronautical and Astronautical Engineering
University of Illinois at Urbana-Champaign
104 South Mathews Avenue
Urbana, Illinois 61801

Final Technical Report
AFOSR Grant 89-0308
for the period 1-September-1989 – 30-September-1991

Prepared for:

Air Force Office of Scientific Research, AFSC
Attention: Dr. Mitat Birkan / NA
Building 410
Bolling Air Force Base, DC 20332-6448

November, 1991

ABSTRACT

A model of a microwave-induced plasma propulsion system has been developed in one dimension for a transverse electric mode (TE_{10}) of operation in a rectangular waveguide. Available experimental data are compared to the computational results for the case of a planar propagating plasma wave and, using a TE_{10} mode-shape approximation, for a wave propagating in a waveguide. Temperature profiles, plasma propagation velocities, velocity profiles, and absorbed power histories are obtained for flow of helium from .5 to 1 atmosphere pressure and 500 to 3000 watts input power at a frequency of 2.45 GHz. The computational results show the observed jumping of the plasma towards the microwave source. Peak plasma temperatures range from 8000 to 9000 K over the input power range. For an input power of 1081.7 W the calculated percentage of power absorbed is approximately 70 percent for the planar case and 40 percent for the waveguide case. Comparisons with experimental data indicate other mechanisms (not involving transient processses), most likely associated with the nonequilibrium behavior of the plasma, are responsible for the disagreement between the model results and the observed plasma propagation velocities.

ACKNOWLEDGEMENT

The authors wish to acknowledge the financial support provided for this research by the Air Force Office of Scientific Research under grant AFOSR-89-0308, Dr. Mitat Birkan, Program Manager.

TABLE OF CONTENTS

LIST OF FIGURES

NOMENCLATURE

A	amplitude of electric field
a	waveguide width
A_c	area of waveguide cross section
b	waveguide height
c	speed of light
c_p	constant pressure specific heat
c_v	constant volume specific heat
$\vec{E}$	electric field
e	total internal energy per unit mass
$\vec{H}$	magnetic field
h	total enthalpy per unit mass
i	$\sqrt{-1}$
P	power
p	pressure
$\vec{q}^c$	conductive heat flux vector
$\vec{q}^r$	radiative heat flux vector
$\vec{R}$	right running electric field wave
$\vec{L}$	left running electric field wave
R_0	amplitude of right running electric field wave
T	temperature
t	time
$\vec{u}$	velocity vector with components {u,v,w}
$\vec{x}$	position vector {x,y,z}
β	phase constant
γ	isentropic exponent

ε	permittivity
ε_0	permittivity of free space
μ	permeability
μ_0	permeability of free space
ρ	density
σ	electrical conductivity
$\vec{\vec{\tau}}$	viscous stress tensor
ω	angular microwave frequency

Subscripts

I	imaginary component
R	real component
r	radial component
x	x component
y	y component
z	axial component

Superscripts and Operators

$\overline{\quad}$	average of variable over time

(This page left blank for two-sided copies.)

1. INTRODUCTION

1.1 OVERVIEW - MICROWAVE PROPULSION

Some of the advanced propulsion systems currently being considered for future space missions are the resistojet, arcjet, ion engines, and laser and microwave electrothermal propulsion systems. Studies conducted of advanced propulsion concepts for both NASA and Air Force missions, such as low-earth orbit transfers and long duration missions, have yielded certain optimum parameters of operation. With current electrical power generation capabilities, propulsion systems with specific impulses in the range of 1000 to 2000 seconds would optimize the payload ratio of these spacecraft (Micci, 1984). Of the advanced propulsion concepts mentioned, microwave electrothermal propulsion systems best suit this range of operation.

Resistojets employ electrothermal heating through electrical resistance in a solid placed in the flow of the propellant. These devices are, therefore, limited by the materials involved and currently achieve a maximum specific impulse of below 385 seconds even when using hydrogen as the propellant (Mueller and Micci, 1989). Arcjets also use electrothermal heating, but do so through use of an electrical arc passing through the fluid. These systems have a specific impulse of approximately 700 seconds for ammonia propellants at high input power levels (Mueller and Micci, 1990). The electrodes are subject to erosion, especially at higher input power levels, and thereby limit the lifetime of such systems. In the study of cathode erosion by Deininger, Chopra, and Goodfellow, the lifetime of a 30 kW-class arcjet was only 573 hours (Deininger, et al., 1989) as compared to the lifetime estimate of 10,000 hours for such mission profiles as orbit transfer and orbit control for the space station (Mueller and Micci, 1990). A propulsion system using arcjets would thus

require backup thrusters adding to the overall mass of the spacecraft. Propulsion devices relying on electrostatic and electromagnetic means have optimum operation at much higher specific impulses and have thrust levels on the order of only a few Newtons.

Most laser thermal propulsion concepts use the laser to optically heat the propellant forming a plasma, or hot gas region. The heated propellant is then accelerated by use of a standard supersonic nozzle configuration. Laser thermal systems could have the laser energy produced elsewhere, such as on the Earth, and beamed to the spacecraft, making for a very low specific mass. Problems arise, however, in focusing, absorption, refraction, and divergence of the beam through the atmosphere. Also, laser systems can suffer from low efficiencies due to radiation losses from the plasma and low energy conversion processes (Jeng and Keefer, 1987). Microwave thermal propulsion devices are also an electrodeless, plasma producing device and have better efficiencies than those of laser systems. Gas absorptivities are higher at microwave wavelengths than at optical wavelengths for temperatures below those yielding significant ionization. This enables operation at lower power levels and thus lower temperatures, thereby eliminating the problems of radiative and ionization losses. Also, microwave conversion efficiencies are higher and the microwave generating devices are less complex (Venkateswaran, et al., 1990).

Microwaves are generally considered to have frequencies ranging from 10^9 to 10^{12} Hz, corresponding to characteristic wavelengths of .3 to .0003 meters. Since these wavelengths can be on the same order as propulsion chamber dimensions, resonance characteristics can be obtained by proper dimensioning of an enclosed waveguide shape. This is the general reasoning behind the use of resonant cavity waveguides. Microwaves are governed by Maxwell's equations and as such have an infinite number of different possible solutions, each of which corresponds to a mode

of propagation in a waveguide. These modes are divided into three classifications according to the fields present in the waveguide when that mode is propagating. These classifications are the TE, TM, and TEM modes. In the TE, or transverse electric, mode there is no longitudinal component of the electric field, but only transverse components of the electric field. In the TM, or transverse magnetic, mode there is no longitudinal component of the magnetic field. A wave with only transverse components of both the electric and magnetic fields is called transverse electric and magnetic, or TEM. The TE and TM modes are further divided by the values of two integers, m and n, used in the expressions for the components of the field. These integers appear as subscripts of TE or TM. Different modes of operation have different frequencies below which there is no propagation of the microwave. This is called the cut-off condition (Fuller, 1969). The lowest, or dominant, mode of operation is usually used in microwave systems through use of a low input frequency. This avoids multiple modes of operation of the microwave fields through the use of the cut-off condition.

Several concepts for microwave propulsion systems have been considered in the past. Micci (1984) groups the various systems into five different categories. In the first, the propellant is passed through a constraining tube located within a waveguide or resonant cavity. This concept suffers from a high temperature located close to the walls of the constraining tube which leads to thermal breakdown. Also, it was found that heat loss by conduction to the walls of the tube was greater than that of the heat convected to the propellant, making such a system undesirable (Micci, 1984). A second setup is referred to as the "coaxial microwave plasmatron". As the name suggests, the microwave energy is introduced through the use of a coaxial line instead of a waveguide. The propellant is introduced upstream of the termination of the center conductor of the coaxial line and the plasma is formed at the end of the coaxial line. Difficulties arise from this concept due to the plasma

region being next to the center conductor (Batenin, et al., 1976a; Batenin, et al., 1975; Batenin, et al., 1976c; Miyake, et al., 1974).

The third and fourth concepts involve the use of a resonant cavity configuration in a cylindrical waveguide. In the filamentary mode, the microwave energy is input at the TM_{01} mode of operation. In this mode shape, the peak of the electric field, and thus the location of the plasma, lies along the centerline of the cylinder. Experimental studies of this system were done in the Soviet Union by Kapitza (1970, 1972) and later by Tishchenko and Zatsepin (1975) and in Japan by Hasegawa, et al. (1975). Theoretical modeling was done by Mieroivich (1972a, 1972b, 1973) and by Asinovskii and Batenin (1973). For the fourth concept, the TE_{01} mode of operation is used instead of the TM_{01}. In this mode shape, the electric field lines are circular and parallel to the longitudinal axis of the resonant cavity cylinder. The maximum of the electric field occurs in a ring lying away from the walls of the cavity. The plasma will then form in a toroidal shape along the ring of maximum electric field strength. Further theoretical and experimental investigation of resonant cavities for use in microwave propulsion systems have been conducted by Whitehair and Asmussen (1984) and Whitehair, et al. (1987) and later by Mueller and Micci (1990) and Venkateswaran, et al. (1990).

The fifth concept involves the absorption of the microwave energy by a plasma region contained within a waveguide serving as a propulsion chamber. In this scheme the plasma propagates toward the source of the microwave energy and must be stabilized by some means. The plasma front then acts similarly to a combustion wave front, heating the propellant which is accelerated out a nozzle. Experimental and theoretical studies relevant to this concept have been conducted by Beust and Ford (1961), Raizer (1972), Batenin, et al. (1973, 1976, 1977), Knecht and Micci (1988), Mueller and Micci (1988, 1989, 1990). The research described in this thesis is of an alternate approach to the computational modeling of the plasma

wavefront concept and shows the results and comparisons of the model to available experimental data.

1.2 OVERVIEW - PLASMA DEPOSITION

Microwave induced plasmas are also ideal for coating applications such as chemical vapor deposition (CVD), thin-film deposition and etching (Asmussen, 1989; Hsu, et al., 1989). Due to their electrodeless nature, the plasma cannot be contaminated by impurities contained in the electrode material. Thus a higher degree of flexibility in the composition of the plasma is possible with respect to the radiation properties. This is of great importance in CVD processes. Microwaves allow for better control of the temperature distribution through variation of the input frequency. Also, manufacturing and lifetime aspects are improved through the use of microwave systems (Offermanns, 1989). Further understanding of the dynamics of the interactions of the gas or gases with the plasma would be beneficial in the optimization of various coating qualities. The following analysis and results, however, focus on the propulsion aspect of microwave induced plasmas, although the model could be similarly applied to model plasmas used in chemical vapor deposition applications.

1.3 MODELING APPROACH

A microwave discharge in a waveguide is observed to propagate towards the source of the power in configurations with no added stabilization techniques. There are four main propagation mechanisms that may be involved. Three mechanisms described in the paper by Bethke and Reuss (1969) for low pressures are gas photoionization due to resonant radiation, electron ionization due to collisions with

energetic electrons and electron diffusion. Myshenkov and Raizer (1971) combined these first two mechanisms as resonant radiation. For pressures closer to atmospheric, the dominant mechanism is heat conduction (Batenin, et al., 1973; Raizer, 1972). Batenin, et al. (1973) also found resonant radiation important for heavy gases at atmospheric pressures. In each case, the particular mechanism causes microwave heating upstream of the existing plasma region causing the plasma to move towards the source of the power and extinguishment of the plasma downstream. The extinguishment develops due to attenuation of the microwaves through the plasma region, and thus, the downstream region cannot maintain the plasma.

Theoretical models of microwave systems have been developed using several different approaches. Analytic solutions of the electromagnetic system have been developed by Myshenkov and Raizer (1972) and Raizer (1972). In each, the equations are solved in the frequency domain, and therefore, assume a frequency dependence of the electric field. Several simplifying assumptions are used such that the particular problem is reduced to an eigenvalue problem for the propagation velocity.

In computational models of electromagnetic field propagation, there are two principle approaches to the problem. In the first approach, the electromagnetic system is solved in the time domain. This puts severe restrictions on the maximum allowable time step. Yee (1966) developed an algorithm for solutions of Maxwell's equations. This model was later improved by Mur (1981) who modified the boundary conditions, and by Goorjian (1990). The work of Venkateswaran, Merkle, and Micci (1990) is based on the algorithm developed by Yee.

In the second modeling approach, the equations are solved in the frequency domain, and thus, the electric field has an assumed frequency dependence. This approach eliminates the problems of the time increment. Rhodes and Keefer (1989)

developed an axisymmetric, two dimensional model for a radio frequency gas heater which can be related to a microwave system. They used the frequency domain and solved the system by use of a complex, electric field vector potential in the SIMPLE algorithm derived from earlier work. In the works of Sforza (1969) and Offermanns (1989), models of the microwave system were developed using series expansion approximations.

The objectives of this research include formulation of an electromagnetic equation system coupled to a full time dependent fluid solution to better model the interactions observed in microwave electrothermal propulsion devices. Among these improvements is the need of a model that will show the observed phenomenon of "hopping" of the plasma within the waveguide. The anomalous values for power absorption between the model of Mueller and Micci (1989) with experimental data (Batenin, et al., 1976b; Mueller and Micci, 1989; Raizer, 1972) must be resolved. Also, it is desired to obtain the optimal input parameters that will result in peak input power absorption by the plasma.

2. THEORETICAL ANALYSIS

2.1 FORMULATION OF THE GOVERNING EQUATIONS

The basic flow geometry in a waveguide of either a rectangular or circular cross section is shown schematically in Figures 1a, 1b, and 2. The plasma front is assumed to be initiated within the waveguide and will propagate toward the microwave source unless some means of stabilization is provided. Thus, we consider a non-steady formulation of the fluid dynamic equations. Since the considered operating pressure is approximately atmospheric and flow or propagation speeds are low - subsonic, the plasma is assumed to be in local thermodynamic equilibrium. Additionally, due to absorption limitations, the plasma ionization fraction is typically less than 0.01, and radiative transfer is assumed negligible based on the results of Mueller and Micci (1989).

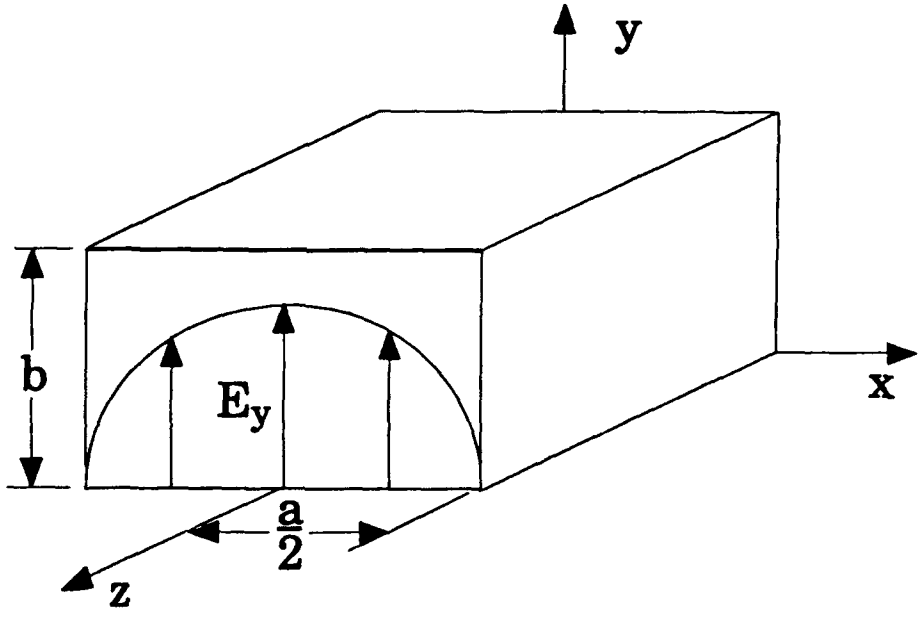

Figure 1a. Coordinate convention for a rectangular waveguide.

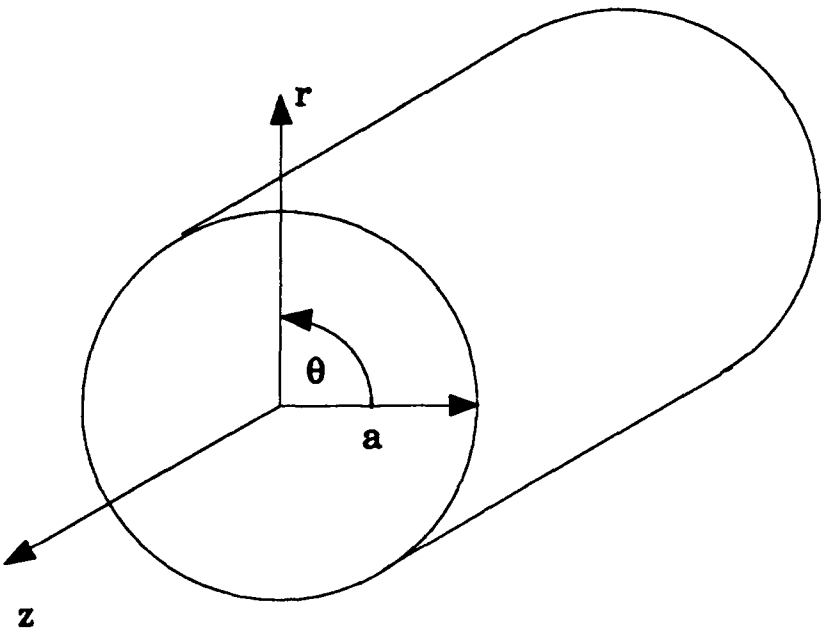

Figure 1b. Coordinate convention for a cylindrical waveguide.

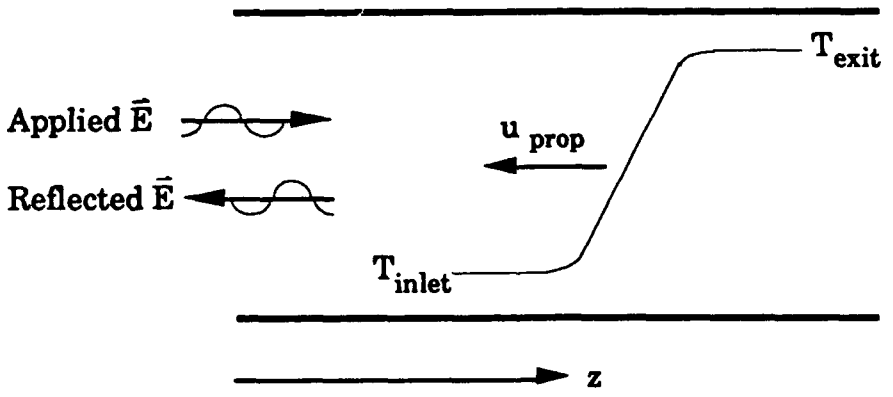

Figure 2. Schematic of plasma propagation in a rectangular waveguide.

The flow is therefore governed by the Navier-Stokes equations for a compressible gas in equilibrium (see, for example, Pai, 1962)

$$\frac{\partial \rho}{\partial t} + \nabla \cdot (\rho \vec{u}) = 0 \qquad (1)$$

$$\frac{\partial \rho \vec{u}}{\partial t} + \nabla \cdot \left(\rho \vec{u}\vec{u} - \vec{\vec{\tau}}\right) = \mu\sigma \overline{\vec{E} \times \vec{H}} \tag{2}$$

$$\frac{\partial \rho e}{\partial t} + \nabla \cdot \left(\rho \vec{u} h + \vec{q}^{c} - \vec{u}\,\vec{\vec{\tau}}\right) = \sigma \overline{\vec{E}^{2}} \tag{3}$$

together with the thermal and caloric equations of state. The time-averaged Lorentz force and Ohmic heating terms in Equations (2) and (3) are determined by the Maxwell equations given below.

$$\frac{\partial \mu \vec{H}}{\partial t} = -\nabla \times \vec{E} \tag{4}$$

$$\frac{\partial \varepsilon \vec{E}}{\partial t} + \sigma \vec{E} - \nabla \times \vec{H} = 0 \tag{5}$$

The above equation uses Ohm's Law to give the current density in terms of the conductivity and the electric field.

For the problem of interest, a single frequency field is assumed to be output by the microwave generator. The medium is assumed to be unmagnetized such that the permeability may be replaced by the permeability of free space and is also assumed to be free of space charge. Both the inverse frequency and wave reflection time scales of the electromagnetic field are readily shown to be much shorter than any of the fluid time scales. Accordingly, a complex representation of the electromagnetic field in the frequency domain is adopted, such that

$$\vec{E}(\vec{x},t) = \mathrm{Re}\left[\left(\vec{E}_R(\vec{x}) + i\vec{E}_I(\vec{x})\right)e^{i\omega t}\right] \tag{6}$$

with a corresponding description for the magnetic field, $\vec{H}$. For the Transverse Electric (TE) mode of operation, in which the axial component of the electric field is zero everywhere, Maxwell's equations are solved for the spatial amplitude of the electric field, $\vec{E}$. For the Transverse Magnetic (TM) mode, Maxwell's equations

would be solved for the spatial amplitude of the magnetic field, $\vec{H}$. The following derivation is for the TE mode of operation.

A multiple scale analysis of the equation was done to determine the relevant terms. Two times, corresponding to the slow time associated with the fluid time scale, t, and fast time associated with the frequency of the input electric field, τ, were employed. Thus, the value of t/τ relevant to the frequencies used was on the order of 10^{-6}. Derivatives with respect to time of ε and σ were found to be negligible in comparison to the remaining terms. Only zeroth order terms are retained. Splitting the resulting equation into real and imaginary parts yields coupled equations for the real and imaginary spatial amplitudes, $\vec{E_R}$ and $\vec{E_I}$. Since we are dealing with the TE mode of operation, however, there is no axial (z) component of the electric field. Thus, the equations may be written as follows.

Real: $$\nabla^2(\vec{E}_R(x,y)) + \omega^2\mu\varepsilon(\vec{E}_R(x,y)) + \omega\mu\sigma(\vec{E}_I(x,y)) = 0 \quad (7)$$

Imaginary: $$\nabla^2(\vec{E}_I(x,y)) + \omega^2\mu\varepsilon(\vec{E}_I(x,y)) - \omega\mu\sigma(\vec{E}_R(x,y)) = 0 \quad (8)$$

Further reduction of the vectors into scalar quantities is done in both the one and two dimensional formulations and shall be discussed in these separate sections.

2.2 BOUNDARY CONDITIONS

The boundary conditions at the inlet and exit of the waveguide for both the one and two dimensional formulations make use of the left and right travelling wave characteristic equations. In the two dimensional formulation, boundary conditions for the wall and centerline are also necessary. These boundary conditions will be discussed in the two dimensional section.

2.2.1 Inlet Boundary Conditions

The electric field at the inlet can be expressed as the sum of the known input electric field, R, which is a right running wave and an unknown reflected electric field, L, which is left running. The characteristic equations for a left and right travelling wave are given below.

$$\frac{\partial \vec{L}}{\partial t} - \frac{\omega}{\beta}\frac{\partial \vec{L}}{\partial z} = 0 \tag{9}$$

$$\frac{\partial \vec{R}}{\partial t} + \frac{\omega}{\beta}\frac{\partial \vec{R}}{\partial z} = 0 \tag{10}$$

The parameter, β, is the phase constant (to be defined subsequently) and is dependent on electromagnetic parameters and mode shape. The input electric field may be written as follows.

$$\vec{R} = \vec{R}_0 \, e^{i(\omega t - \beta z)} \tag{11}$$

In the two dimensional case, $\vec{R}_0$ is a function of the radius. Solving for $\vec{L}$ in terms of $\vec{R}$ and $(\vec{E}_R + i\vec{E}_I)$ and substituting into the left running wave characteristic equation yields

$$i\beta(\vec{E}_R + i\vec{E}_I) - \frac{\partial(\vec{E}_R + i\vec{E}_I)}{\partial z} = i\,2\vec{R}_0\beta e^{-i\beta z} \tag{12}$$

At the inlet, the conductivity is assumed to be zero so there is no attenuation of the wave. This assumption holds as long as the inlet temperature stays below approximately 3000 K. The angular frequency, ω, is assumed to be a known input. The amplitude of the input electric field, R_0 (V/m), is dependent on the analytic solution, the averaged input power, and the waveguide dimensions which are all related by the power density equation:

$$\overline{P_{input}} = \int \overline{\vec{E} \times \vec{H}}\, dA_c \tag{13}$$

The term A_c refers to the area of the waveguide cross section. Expressions for the magnetic field, $\vec{H}$, in terms of the electric field, $\vec{E}$, are developed from Maxwell's equations and used in the Equation (13).

2.2.2 Exit Boundary Conditions

At the exit a non-reflective boundary condition is employed. Here the electric field must satisfy the characteristic equation for a right running wave.

$$\frac{\partial (\vec{E}_R + i\vec{E}_I)}{\partial t} + \frac{\omega}{\beta} \frac{\partial (\vec{E}_R + i\vec{E}_I)}{\partial z} = 0 \tag{14}$$

It should be noted, however, that once the plasma has formed, there is no transmittance of the wave past the exit due to attenuation of the wave.

2.3 COUPLING TERMS

For the energy equation, the coupling involves the term $\vec{E}^2$. Since the frequency domain is employed, the Ohmic heating term must be averaged over a period of oscillation. Returning to the time dependent mode and averaging over a period of oscillation, it can be shown for both the one and two dimensional cases that

$$\overline{\vec{E}^2} = \frac{1}{2}\left(\vec{E}_R^{\,2} + \vec{E}_I^{\,2}\right) \tag{15}$$

The coupling in the momentum equation is due to $\vec{E}$ x $\vec{H}$. Using Maxwell's equations, relations for the magnetic field in terms of the electric field components

are developed. The cross product is averaged over a period of oscillation like that of the E^2 term. The resulting equation is different for the one and two dimensional formulations and so will be described in each section.

2.4 ONE DIMENSION

A one dimensional analysis can be used to approximate the solution in a rectangular waveguide for the lowest TE mode of operation, the TE_{10} mode. For this case, the only non-zero component of the electric field is the y component (see Figure 1). Thus, E_R and E_I become scalar quantities representing the real and imaginary y-components of the electric field. In matrix form the coupled equations may be written as follows.

$$\begin{bmatrix} \left(\frac{\partial^2}{\partial z^2} + \omega^2\mu\varepsilon\right) & \omega\mu\sigma \\ -\omega\mu\sigma & \left(\frac{\partial^2}{\partial z^2} + \omega^2\mu\varepsilon\right) \end{bmatrix} \begin{bmatrix} E_R \\ E_I \end{bmatrix} = \begin{bmatrix} 0 \end{bmatrix} \tag{16}$$

2.4.1 Boundary Conditions

The simplest form of a one dimensional propagating wave is that of a plane wave. For a propagating plane wave, the incoming electric field is given by

$$R = A e^{i(\omega t - \beta z)} \tag{17}$$

where A, the amplitude (V/m), is a real constant. The phase constant, β, is given by the relation

$$\beta = \omega\sqrt{\mu\varepsilon}. \tag{18}$$

Using Maxwell's equations, an expression for the x-component of the magnetic field may be developed in terms of R.

$$H = \frac{A}{\sqrt{\mu / \varepsilon}} e^{i(\omega t - \beta z)} \tag{19}$$

Using the power density expression in Equation (13) and the dimensions a and b for the width and height of the waveguide, the expression for A becomes

$$\frac{\overline{P_{input}}}{a\,b} = \frac{1}{2} \frac{A^2}{\sqrt{\mu / \varepsilon}}. \tag{20}$$

The inlet boundary condition then employs these parameters in Equation (12).

For a TE_{10} mode wave propagating in a rectangular waveguide, R is given by the following expression (Fuller, 1969).

$$R = A\left[\omega \sqrt{\mu\varepsilon}\, \frac{a}{\pi} \cos\left(\frac{\pi x}{a}\right)\right] e^{i(\omega t - \beta z)} \tag{21}$$

This two dimensional form is used in Equation (13) by taking the peak value of the cosine term. In this derivation it is therefore assumed that the wave maintains the sinusoidal shape across the x cross section. The two dimensionality also effects the waveguide phase constant, β, and produces a cut-off condition, below which no wave is propagated down the waveguide. In general, for a TE_{mn} mode, β is given by

$$\beta = \sqrt{\omega^2 \mu\varepsilon - \left(\frac{m\pi}{a}\right)^2 - \left(\frac{n\pi}{b}\right)^2} \tag{22}$$

where a is the x-dimension and b is the y-dimension of the waveguide (Fuller, 1969). For the TE_{10} mode, β thus becomes

$$\beta = \sqrt{\omega^2 \mu\varepsilon - \left(\frac{\pi}{a}\right)^2}. \tag{23}$$

Using the assumed sine wave shape, the second derivative of x resulting from the Laplacian in the two dimensional equations can be replaced with a constant value.

$$\frac{\partial^2}{\partial x^2} E = -\left(\frac{\pi}{a}\right)^2 E \tag{24}$$

Thus, Equation (24) alters the original equation matrix given in Equation (16).

$$\begin{bmatrix} \left(\frac{\partial^2}{\partial z^2} + \omega^2\mu\varepsilon - \left(\frac{\pi}{a}\right)^2\right) & \omega\mu\sigma \\ -\omega\mu\sigma & \left(\frac{\partial^2}{\partial z^2} + \omega^2\mu\varepsilon - \left(\frac{\pi}{a}\right)^2\right) \end{bmatrix} \begin{bmatrix} E_R \\ E_I \end{bmatrix} = \begin{bmatrix} 0 \end{bmatrix} \tag{25}$$

Similar to the plane wave propagating case, an expression may be developed for the amplitude of the magnetic field, H, in terms of the known input electric field amplitude, R. The value of A may then be evaluated using the expression for power density in Equation (14).

$$\frac{\overline{P_{input}}}{a\,b} = \frac{A^2}{2\mu c}\left[\omega\sqrt{\mu\varepsilon}\,\beta\frac{a^2}{\pi^2}\overline{\cos^2\left(\frac{\pi x}{a}\right)}\right] = \frac{A^2}{2\mu c}\left[\omega\sqrt{\mu\varepsilon}\,\beta\frac{a^2}{\pi^2}\frac{1}{2}\right] \tag{26}$$

As mentioned in the general discussion, the exit boundary for both the planar and waveguide solutions employs the characteristic equation for a right travelling wave to ensure a non-reflective condition.

2.4.2 Coupling Terms

Recall that the coupling to the energy equation is given by Equation (15). For the one dimensional case, the magnetic field consists of an x-component and a z, or

axial, component. Thus, the cross product used in the power density relation becomes

$$\overline{\vec{E} \times \vec{H}} = \frac{1}{2}(E_R H_R + E_I H_I) \tag{27}$$

where the terms H_R and H_I refer to the x-component of the magnetic field. Using Maxwell's equations, these magnetic field components may be expressed in terms of the electric field components as follows.

$$H_R = -\frac{1}{\mu\omega}\frac{\partial E_I}{\partial z} \quad ; \quad H_I = \frac{1}{\mu\omega}\frac{\partial E_R}{\partial z} \tag{28a, 28b}$$

2.5 TWO DIMENSIONS - AXISYMMETRIC WAVEGUIDE

To solve the equation system in a circular waveguide, a two dimensional axisymmetric analysis is posed. The lowest TE mode of operation which has an axisymmetric propagation is the TE_{01} mode. Recall that by definition there is no axial component of the electric field. Since the solution is assumed to be axisymmetric, there can be no angular dependence for either the radial or angular electric field components. Furthermore, the radial component can be shown to be zero by the following Maxwell's relation.

$$\nabla \cdot (\varepsilon E) = \frac{1}{r}\frac{\partial(r\,\varepsilon E)}{\partial r} = 0 \tag{29}$$

Thus, the radial component of the electric field must be a constant and, due to the centerline condition, the constant is zero (see Figure 1b).

In the matrix equations, therefore, E_R and E_I are scalar quantities referring to the angular component of the electric field.

Real:
$$\left[\frac{1}{r}\frac{\partial}{\partial r}\left(r\frac{\partial}{\partial r}\right)+\frac{\partial^2}{\partial z^2}\right](E_R)+\omega^2\mu\varepsilon(E_R)+\omega\mu\sigma(E_I)=0 \tag{30}$$

Imaginary:
$$\left[\frac{1}{r}\frac{\partial}{\partial r}\left(r\frac{\partial}{\partial r}\right)+\frac{\partial^2}{\partial z^2}\right](E_I)+\omega^2\mu\varepsilon(E_I)-\omega\mu\sigma(E_R)=0 \tag{31}$$

For values of small r the radial derivative may lead to computational error due to the 1/r term. The problem with small values of r can be avoided by assuming a non-radial characteristic of the equations, and approximating the input electric field by either a symmetrically shaped wave (sine wave) or by using this sine wave approximation for small values of r. The dependent term in this approximation is then y instead of r and the equations become similar to the two dimensional equations for a rectangular waveguide. For the chosen axisymmetric propagation mode (TE_{01}), a sine wave approximates the analytic solution very well. An approximation factor similar to that involved in the 1-D solution must be added to maintain the proper propagation characteristics. The exact character will be discussed along with the boundary conditions.

2.5.1 Boundary Conditions

For a circular waveguide, the incoming TE_{01} electric field is given by Equation (31)

$$R = A\left[\omega\sqrt{\mu\varepsilon}\,\frac{a}{3.83}\,J_0'\left(3.83\frac{r}{a}\right)\right]e^{i(\omega t-\beta z)} \tag{32}$$

where J_0' is the derivative of the Bessel function J_0 with respect to r, and a is the waveguide radius (Fuller, 1969). For this case, the phase constant is given by the following equation.

$$\beta = \sqrt{\omega^2 \mu\varepsilon - \left(\frac{3.83}{a}\right)^2} \tag{33}$$

As mentioned, the Bessel function can be approximated by a sine wave of amplitude 27.86.

$$R = A\left[\omega\sqrt{\mu\varepsilon}\,\frac{a}{3.83}\left(27.86\,\sin\left(\frac{\pi y}{a}\right)\right)\right] e^{i(\omega t - \beta z)} \tag{34}$$

Since the Laplacian of this function does not lead to β^2, and thus, the original equation set is not satisfied, a correction term must be added to account for the difference. The matrix equations then become as follows.

real:
$$\left[\frac{\partial^2}{\partial y^2} + \frac{\partial^2}{\partial z^2}\right](E_R) + \omega^2\mu\varepsilon(E_R) + \omega\mu\sigma(E_I) = 0 \tag{35}$$

Imaginary:
$$\left[\frac{\partial^2}{\partial y^2} + \frac{\partial^2}{\partial z^2}\right](E_I) + \omega^2\mu\varepsilon(E_I) - \omega\mu\sigma(E_R) = 0 \tag{36}$$

The relation for A from the power density equation then becomes

$$\frac{\overline{P_{input}}}{\pi a^2} = \frac{A^2}{2\mu c}\left[\omega\sqrt{\mu\varepsilon}\,\beta\left(\frac{a}{3.83}\right)^2 \overline{\left(27.86\,\sin\left(\frac{\pi y}{a}\right)\right)^2}\right]. \tag{37}$$

As in the 1-D rectangular case, these parameters are used in Equation (12) for the inlet boundary condition. Also, the exit boundary uses the characteristic equation for a right travelling wave given in Equation (14) and thereby only accounts for axial propagation out of the waveguide.

In the two dimensional case it is necessary to pose boundary conditions for the wall and the centerline of the waveguide. For the method developed, these boundary conditions are very simple. Using the assumption that the wall is a perfectly conducting surface, the electric field must be zero at the wall. Also, the

character of the input electric field in the axisymmetric, TE_{01} mode places the restriction that the electric field is zero at the centerline.

2.5.2 Coupling Terms

As in the case of the 1-D formulation, the energy equation coupling term is given by Equation (15). For the two dimensional, axisymmetric case, the magnetic field consists of an angular component and an axial component. Thus, the cross product used in the power density relation has both an axial component and a radial component.

$$\overline{\vec{E} \times \vec{H}_z} = \frac{-1}{2}(E_R H_{rR} + E_I H_{rI}) \tag{38}$$

$$\overline{\vec{E} \times \vec{H}_r} = \frac{1}{2}(E_R H_{zR} + E_I H_{zI}) \tag{39}$$

The terms H_{rR} and H_{rI} refer to the radial component of the magnetic field while the terms H_{zR} and H_{zI} refer to the axial components. Using Maxwell's equations, these magnetic field components may be expressed in terms of the electric field components as follows.

$$H_{rR} = \frac{1}{\mu\omega}\frac{\partial E_I}{\partial z} \quad ; \quad H_{rI} = -\frac{1}{\mu\omega}\frac{\partial E_R}{\partial z} \tag{40a, 40b}$$

$$H_{zR} = -\frac{1}{\mu\omega}\frac{\partial E_I}{\partial y} \quad ; \quad H_{zI} = \frac{1}{\mu\omega}\frac{\partial E_R}{\partial y} \tag{41a, 41b}$$

2.6 COMPUTATIONAL MODEL

The equations for the one dimensional formulation posed in the previous sections are solved implicitly using central differences for the complex amplitudes,

E_R and E_I, by matrix inversion over the grid domain. This approach eliminates the need for iteration of the final electromagnetic solution at each time interval. The local values of the electric field are then used explicitly in the unsteady, compressible Navier-Stokes equations for equilibrium flow. The fluid solution is found using the one-dimensional version of the time accurate, finite volume method developed by Ridder and Beddini (1989). The fluid used, helium, is assumed to behave as a perfect gas in local thermodynamic equilibrium (LTE). This modeling system sets no restrictions on the location of the plasma. There is no Courant-Freidrichs-Lewy (CFL) number restriction in the normal sense. The time step is limited only by truncation error involved in resolving the scales of interest (principally the plasma wave thickness and propagation speeds), and thus the time step may utilize a CFL number of order 10^2 or more for the posed problem. This is a great advantage over schemes solved in the time domain which must use time increments corresponding to the frequency of microwave oscillation which is much smaller than any of the fluid time scales. The grid is restricted by the thickness of the plasma wavefront. The grid cells, therefore, have a maximum increment beyond which the electric field is not accurately defined. For the range of inputs used in this work, the time increment was 10^{-3} seconds and the grid spacing was 10^{-3} meters, corresponding to a CFL number of approximately 600. In this way the plasma-fluid system is modeled by a time accurate approach that allows for easy variation of the input parameters to study the effects.

3. RESULTS AND DISCUSSION

The conditions and parameters of the present investigation are chosen to correspond with the prior experiments of Batenin, et al. (1977) and Mueller and Micci (1989). Both studies used similar arrangements, although the specific conditions of the latter experiment are for a TE_{10} mode at 2.45 GHz. The waveguide cross section is 7.214 x 3.404 cm^2. Both experiments also used helium as a test medium, and an inlet, cold gas temperature of 300 K is assumed.

As indicated by the classical approximate analysis of Raizer (1972), the plasma propagation and absorption conditions are strongly dependent on transport, thermodynamic and electrodynamic properties. A literature review was conducted to determine the data, or the most appropriate methods for developing data, for helium properties over the approximate pressure range of 0.5 to 1.0 atmospheres and temperature range of 300 to 10000 K. Values of parameters such as viscosity, thermal conductivity, permittivity, and conductivity are discussed and graphically presented in the Appendix.

With one exception that shall be discussed subsequently, all calculations to be presented involve artificially "igniting" the plasma near the exit of the waveguide by providing an enhanced electrical conductivity corresponding to a temperature of 6800 K. The plasma wave is then monitored as it moves to the inlet of the waveguide through essentially stagnant gas. The length of the waveguide used is one meter, thereby ensuring adequate monitoring distances of several free space wavelengths (~0.2 m). The number of axial nodes employed in the calculations was nominally 1000, and preliminary sensitivity studies were performed to ensure that this number was sufficient to accurately resolve the thin plasma wave thickness (~5 cm) obtained at higher input power levels (3 kW). The calculations shown represent

the solutions for a planar propagating wave and for a TE_{10} mode wave propagating in a waveguide. Recall that the cross sectional characteristics in the waveguide were assumed to remain the same as in the analytic solution for propagation in a waveguide containing no plasma.

Figure 3 shows the variation with time of the plasma propagation velocity. The seeming thickness of the lines is due to the interpolation scheme used to find the plasma wavefront. The sinusoidal shape shows the effects of the "peaks" and "valleys" of the sinusoidally varying electric field and the observed phenomenon of the plasma jumping from peak to peak. As the plasma approaches a peak of the electromagnetic power the propagation velocity increases. The plasma is most stable at the peak, accounting for the slower propagation as the plasma moves off the peak of the electric field. The figure also shows that the plasma propagation

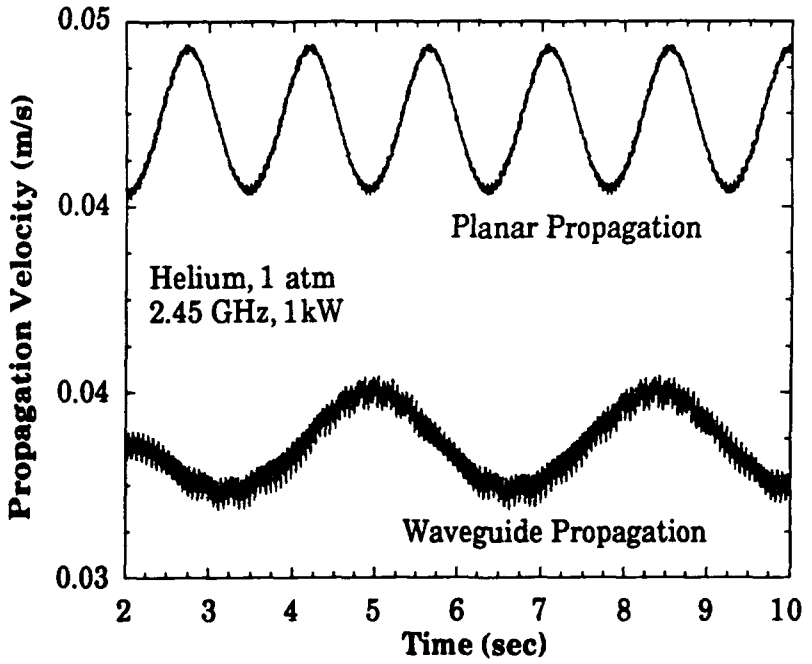

Figure 3. Plasma propagation velocity time histories for helium at one atmosphere and 1000 W input power.

using the waveguide corrections is lower than that of the planar propagating wave. Also, the two cases show different wavelengths of oscillation and amplitudes.

Figure 4 shows a representative electric field distribution for the waveguide case at a time of 5.0 seconds corresponding to a maximum in the propagation velocity. As is evident, the input field is totally attenuated in the results over a distance of approximately 10 cm. The attenuation is achieved by both absorption and reflection which will be discussed subsequently. Negligible transmission under these conditions was also reported in the experiments of Batenin, et al. (1976b).

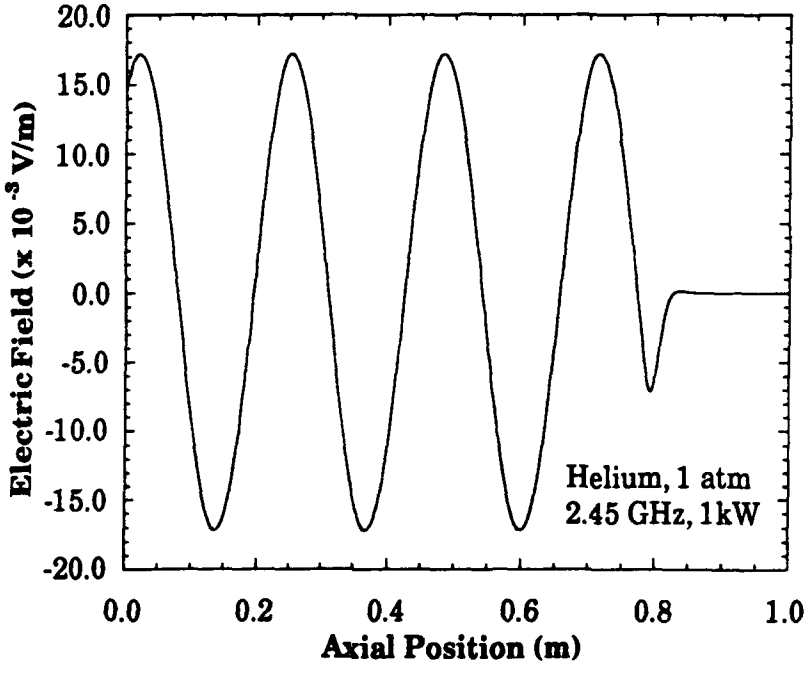

Figure 4. Representative electric field distribution for helium at one atmosphere and 1000 W input power for the waveguide case.

Figure 5 shows the dependence of averaged plasma propagation velocity on input power for the two cases of the present results as well as the experimental and theoretical results of Mueller and Micci (1989). Neither model is able to reproduce the pronounced dependence on input power observed. The jump in the

experimental data near 1500 W may be attributable to a different propagation mode due to resonant radiation (Batenin, et al., 1973; Mueller and Micci, 1989), but the lower power values do not agree or show a similar power dependence. The one dimensional model developed by Mueller and Micci (1988) for a planar propagating wave shows much lower plasma propagation velocities in comparison to the present results, which vary from approximately 0.2 to 2.0 cm/sec over the same power range. Their results also show less dependence on input power. This discrepancy may be partially due to differing values for the properties of the fluid such as conductivity and permittivity. The importance of the properties shall be discussed later. Their model also approximates the reflection of the electric field from the plasma wave. Continuous reflection, included in the present formulation, allows for spatially continuous reabsorption of electric field waves reflected from within the initial regions of the plasma, yielding steeper temperature gradients.

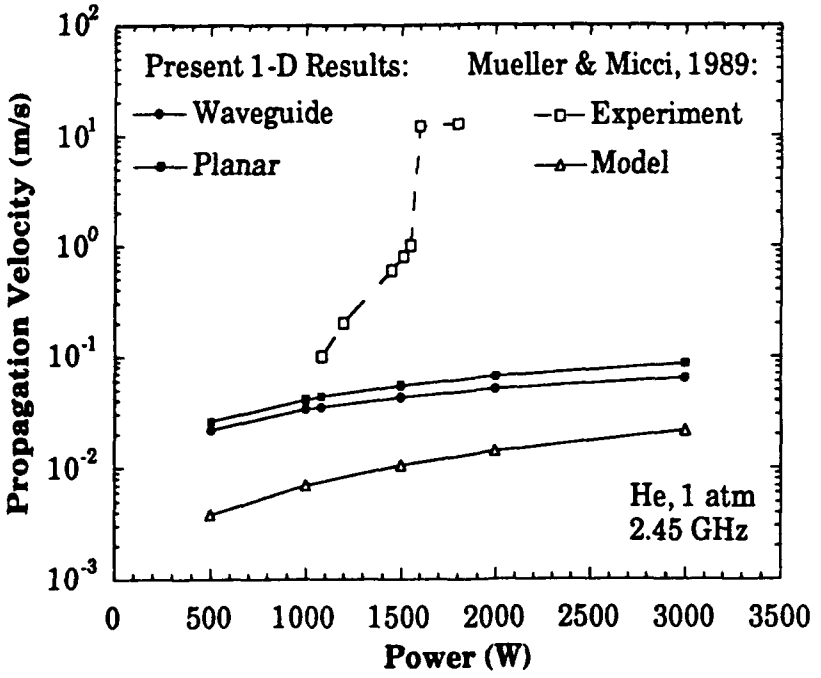

Figure 5. Plasma propagation velocity for helium at 1 atmosphere pressure and 500 to 3000 W input power.

Figure 6 shows the dependence of averaged plasma propagation velocity on the static pressure within the chamber, or waveguide, along with the experimental results of Batenin, et al. (1977) and Mueller and Micci (1989). Both the planar and waveguide cases fail to show the pronounced pressure dependence of the experimental data. The calculated pressure dependence of the plasma propagation velocity is approximately p^{-1}. The experimental data, however, are better represented by an exponential pressure dependence, i.e. , $u_{prop} \sim \exp(\alpha p)$. The exponential factor, α, is approximately - 4.7 for Batenin, et al. and approximately - 6.9 for Mueller and Micci. The exponential pressure dependence of the experimental data further suggests that the assumption of LTE is incorrect, even at these relatively high pressures. Non-LTE behavior in relation to microwave plasmas has been indicated in the spectroscopic data of Batenin, et al. (1977, 1976c) and Mueller and Micci (1989). In this latter study, electron temperatures were measured to be approximately 13,000 K compared to calculated ion and neutral particle temperatures of approximately 8,000 K for input powers of 500 to 3000 W. Recently, non-LTE behavior has been discussed theoretically and experimentally in the region downstream of a radio-frequency discharge in argon (Owano, et al., 1991). The observed electron concentrations at one atmosphere and 9000 K were substantially higher than equilibrium levels.

More insight as to the extent of non-equilibrium behavior is obtained from a theoretical analysis which follows the spirit of those done by Raizer but with further simplifications. The Ohmic heating term is approximated by the maximum electric field amplitude and the values of electrical and thermal conductivity are based on the plasma temperature. A simple scaling analysis of the energy equation using the assumption of total absorption leads to the following relation:

$$u_{prop} \cong \frac{1}{\rho_{inlet}} \frac{E_{max}}{c_{p,\,inlet}} \left(\frac{\sigma_{exit}\, k_{exit}}{2\,(T_{exit} - T_{inlet})} \right)^{\frac{1}{2}}.$$

For an input power of 1000 W and helium at one atmosphere and 300 K, the exit temperature is 8000 K. The value of E_{max}, which relates to the parameter A in the theoretical formulations, is approximately 1.75×10^4 V/m for a planar propagating plasma wave. The density at the inlet is taken to be .16 kg/m^3 and the value of c_p is approximately 5200 J/kg/K. At 8000 K, the electrical conductivity is 0.65 mho/m and the thermal conductivity is 1.85 W/m/K. These values yield a propagation velocity of approximately 0.2 m/s, which is in order-of-magnitude agreement with the present calculations.

Due to the present assumptions, the thermal conductivity is independent of pressure, and the electrical conductivity has a weak pressure dependence within the range 0.4 to 1.0 atmospheres. The theoretical dependence of the plasma propagation is, therefore, mainly due to the density, giving a pressure dependence of approximately p^{-1} for equilibrium conditions. The experimental data suggests a higher pressure dependence for the electrical conductivity. Furthermore, it can be inferred that if the thermal propagation mechanism is valid, then the electrical conductivity, and thus the electron number density, is an order of magnitude higher than the LTE value.

Although a non-LTE model should be incorporated first, another possibility of the anomalous behavior is that the thermal propagation mechanism may not be valid for these pressures. Batenin, et al. (1976b) suggests that the propagation mechanism is not clearly defined between heat conduction and resonance-radiation diffusion. If radiation were important, the thermal conductivity would increase, possibly giving better quantitative results.

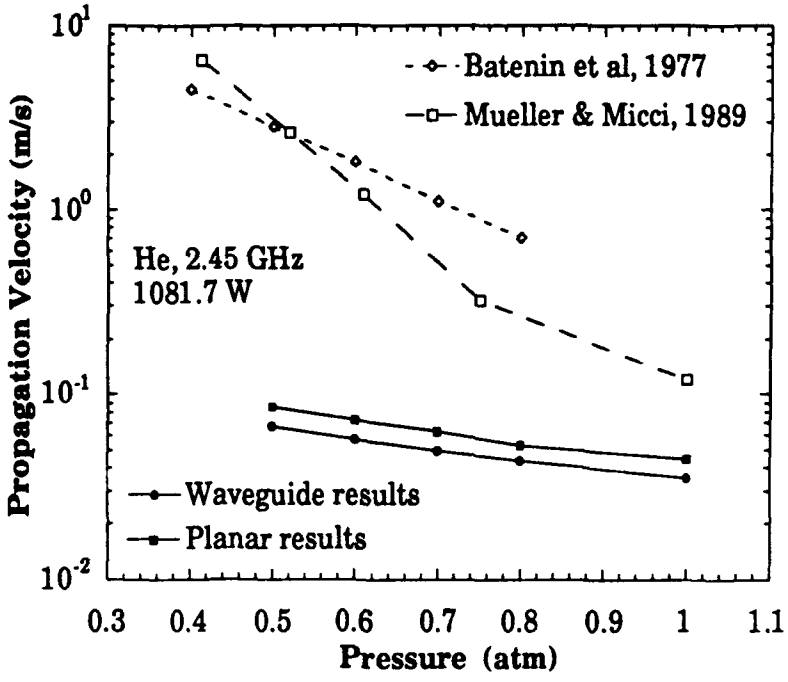

Figure 6. Plasma propagation velocity for helium at 1081.7 W and 0.5 to 1.0 atmosphere chamber pressure.

Figure 7 shows the averaged chamber, or waveguide, exit velocity over a range of input power levels for the two cases of the present results along with the theoretical results of Mueller and Micci (1989). In the theoretical work of Mueller Micci (1989) the exit velocities were calculated for both one and ten atmospheres of chamber pressure. Qualitative agreement exists between the models for the overall decrease of exit velocities for increasing pressure. The present results, however, show higher exit velocities and greater dependence on the input power. Figure 8 shows the dependence of the averaged chamber exit velocity on pressure for the two cases of the present results. Note that the results for the waveguide corrected solution in both Figure 7 and 8 are less than that of the planar results, although each shows the same power and pressure dependence.

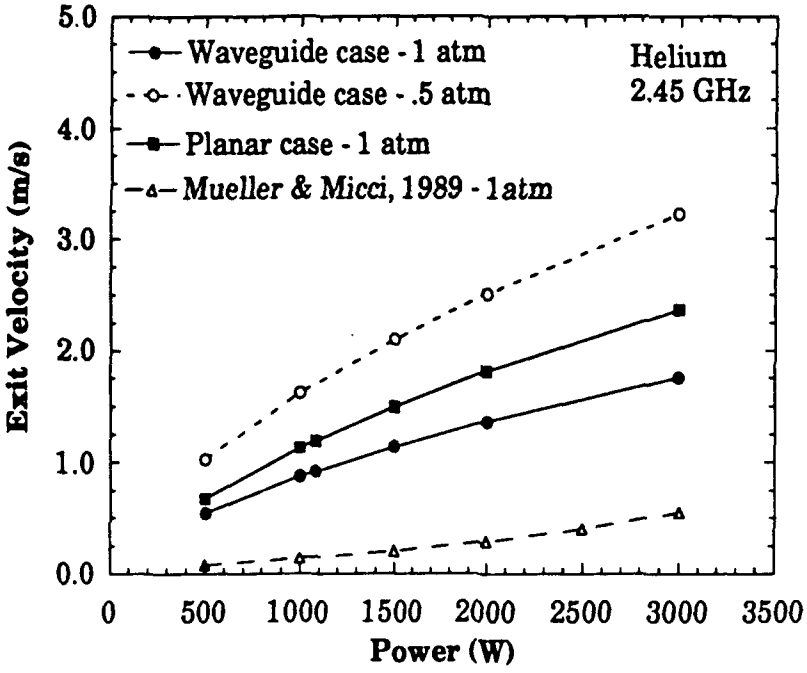

Figure 7. **Chamber exit velocity for helium at .5 and 1 atmosphere pressure and 500 to 3000 W input power.**

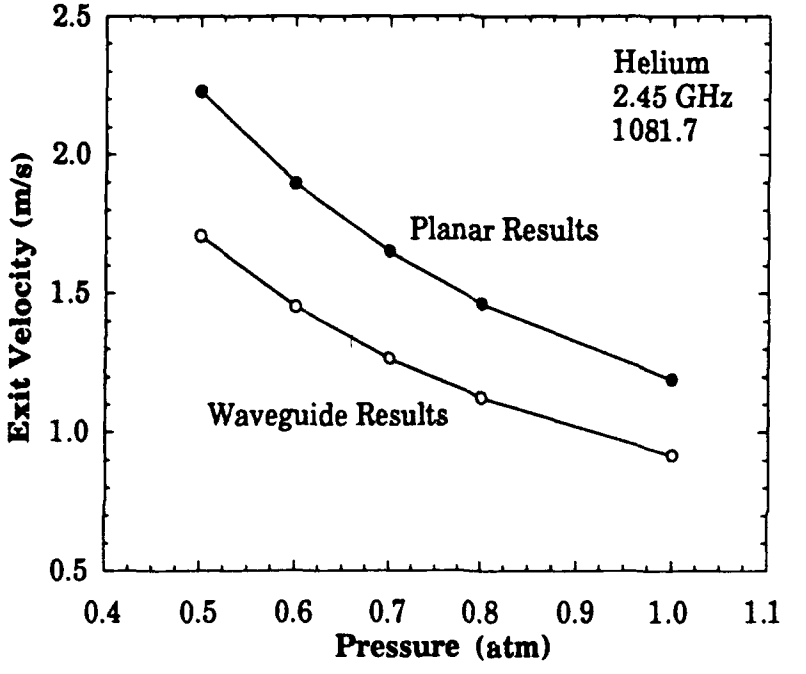

Figure 8. **Chamber exit velocity for helium at .5 to 1 atmosphere chamber pressure.**

Figure 9 shows the temperature profiles of the propulsion chamber (waveguide) over a range of input power levels for the waveguide corrected case. All profiles were taken at the same time level (5 seconds). Initial startup acoustic disturbances were small and quickly died away (less than 2 seconds in real time for the lowest power level). The calculations show a steep wavefront. For the 500 W case, the wavefront is approximately twenty centimeters across for a temperature change of 7500 K. The planar propagating results are very similar to the case shown, having slightly wider plasma wavefront thicknesses and slightly lower peak temperatures. The values of plasma wavefront thickness are much smaller than predicted by the model of Mueller and Micci (1988), especially for the 500 W case. The peak temperatures of the current work are also approximately 1000 K higher, again suggesting partial absorption of the reflected field as a source of the difference.

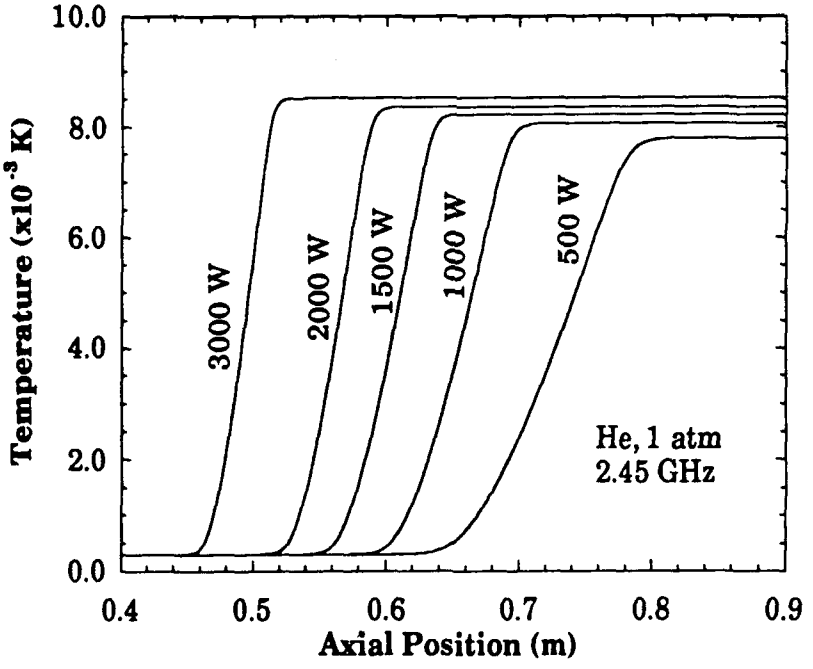

Figure 9. Temperature profiles for helium at 1 atmosphere and 500 to 3000 W input power.

The absorbed and reflected power levels in the present calculations were obtained by two methods. For the reflected power, the value of E x H was calculated at the inlet using Equation (27) and compared with the input value from Equation (14). For the absorbed power, the integral of the Ohmic heating term, σE^2, was calculated using Equation (16). The two values agreed within three percent of each other. Figure 10 shows the time history of the percentage of input power absorbed by the plasma. As in the case of the time history of propagation velocity, the absorbed power cycles sinusoidally as the plasma moves through the regions of the peak electric field. The percent of power absorbed for the waveguide case is less than that of the planar propagating case. This is due to the assumption of the sinusoidal cross sectional shape as opposed to a plane wave at peak electric field strength. Also, note the longer wavelength and smaller amplitude of oscillation in the waveguide case just as in the propagation time history results.

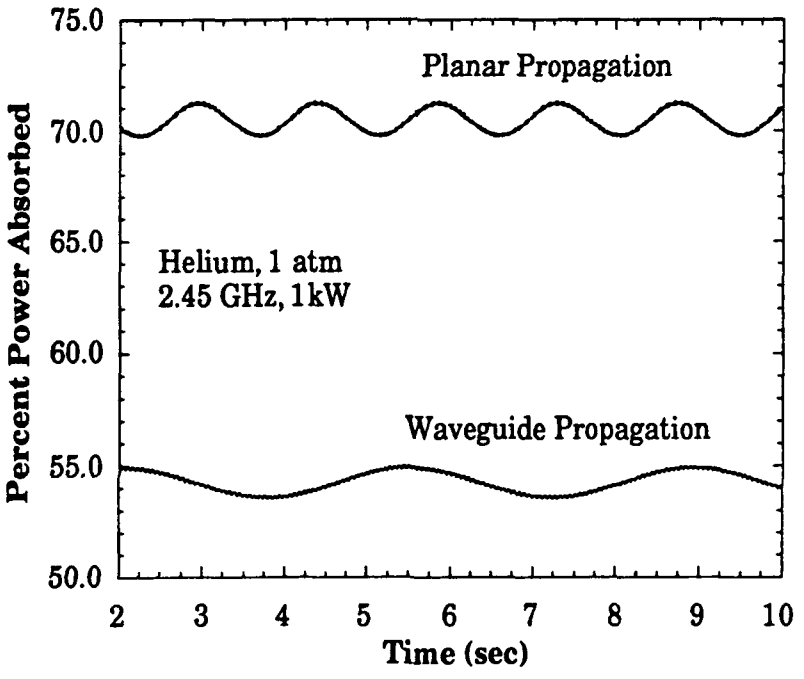

Figure 10. Absorbed power history for helium at 1 atmosphere and 1000 W input power.

Figures 11 and 12 show the percentage of input power absorbed over a range of input powers and pressures. In the experimental results of Mueller and Micci (1989) for helium at one atmosphere, the power absorption was within the middle 60 to lower 70 percent range. This would suggest better agreement of the planar results to the experimental work than that of the waveguide corrected case. For helium at 1081.7 W, the absorption decreased from approximately 65% at .25 atmospheres to 60% at one atmosphere. Thus, both calculations and experiment yield little dependence on pressure, and overall agreement in absorbed and reflected power levels is considered good.

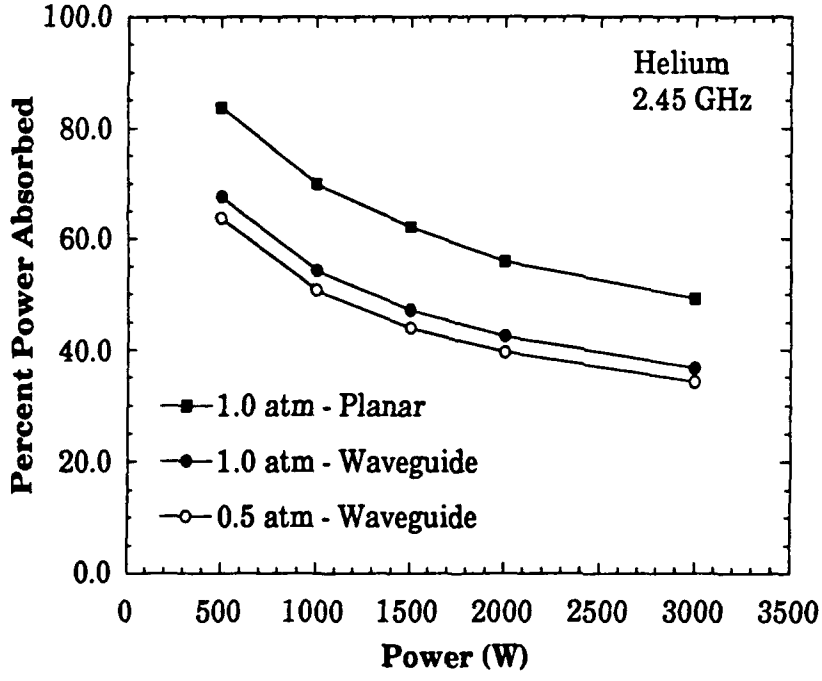

Figure 11. Absorbed power for helium at .5 and 1 atmosphere, 500 to 3000 W input power.

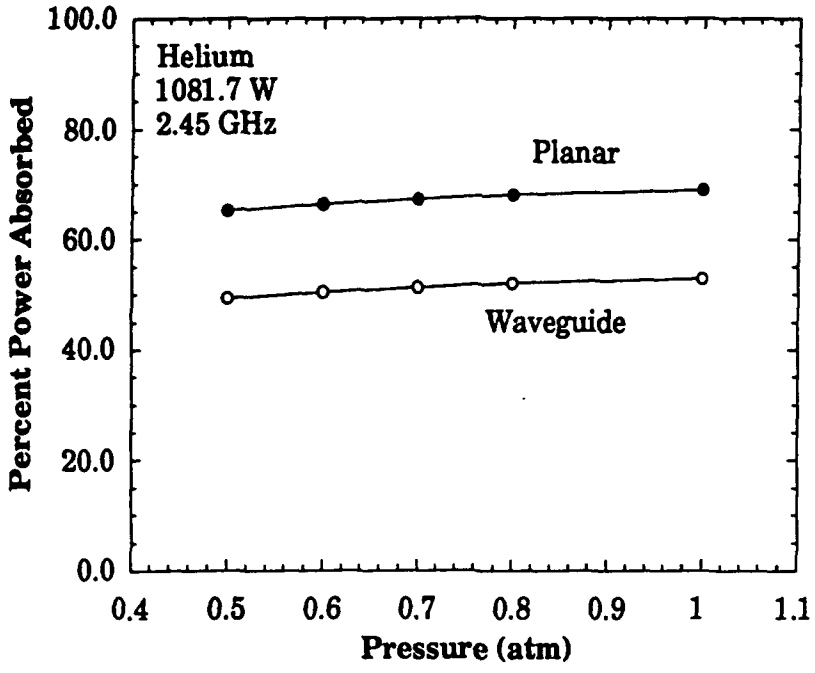

Figure 12. Absorbed power for helium at .5 to 1 atmosphere chamber pressure.

Further calculations have been done to ascertain the affects of a low speed, stabilizing inlet mass flux. Using a previous calculation of the propagation speed to determine the proper mass flux necessary, it was possible to stabilize the plasma near a location of maximum power absorption. This stabilization, however, is greatly dependent on the pressure and temperature remaining at fixed levels and a non-varying flow speed, making simple mass flux control unfeasible for plasma stabilization. Besides the use of a bluff body to stabilize the plasma in the recirculating regions (Mueller and Micci, 1990), it is believed that the use of a simple divergently-shaped chamber liner (made of dielectric material) could also stabilize the discharge over a range of operating conditions. Although the properties of the flow would vary somewhat, the plasma would simply move up the diverging duct toward increasing flow velocity, or down the duct toward slower velocities, to that position where the inlet mass flux stabilizes the plasma.

4. CONCLUSIONS

A computational model of a microwave induced plasma propulsion system is developed in one dimension for the TE_{10} mode of operation in a rectangular waveguide. The propellant used, helium, is assumed to behave as a perfect gas in local thermodynamic equilibrium. The effects of radiation are neglected due to the relatively low temperatures and ionization fraction of the plasma. Also, the electric field is assumed to reach a steady solution at each time interval based on the known frequency of oscillation. Maxwell's equations are solved implicitly using central differences for the complex amplitudes of the electric field at each grid cell center. The electric field is coupled with the Navier-Stokes equations which are solved by a time-accurate finite volume method. This model sets no restrictions on the location of the plasma. The time step is limited only by accuracy in resolving features such as wave thickness and propagation speed. The grid is restricted only in that the cells must be small enough to accurately resolve the plasma wavefront. Two approaches are developed in the modeling of the electric field. In the planar case, the electric field is assumed to be a planar propagating wave. In the waveguide case, the electric field is assumed to have a sinusoidal cross sectional shape and appropriate corrections on the phase constant due to waveguide propagation are employed.

The model was capable of stabilizing the plasma at a fixed axial position by adjusting the inlet mass flux. However, owing to the eigenvalue behavior of the mass flux, this approach to stabilization would not be adequate in practice. It is suggested that a simple diverging duct could be used for stabilization which would hold the plasma at the proper location for countering the mass flux, even if the mass flux varies to some degree.

A simple scaling analysis of the dependence of the plasma propagation velocity on pressure is calculated. The theoretical analysis, based on the property formulations shown in the Appendix, suggests a dependence of approximately p^{-1} on the propagation velocity. The experimental data, however, show an exponential dependence on pressure. This suggests that the LTE assumption is incorrect at atmospheric pressure and as such, a non-equilibrium thermodynamic analysis is required. Also, it would be of great interest to have experimental data at higher pressures (on the order of 10 atmospheres) to examine under what conditions, if any, the LTE assumption is valid.

The model does show the observed phenomenon of the jumping of the plasma towards the microwave source due to the peaks of electric field strength. The percentage of input power absorbed calculated by the model agrees fairly well with experimental results. The planar case shows better quantitative agreement than the waveguide case. Neither case agrees with the experimentally shown pressure dependence.

Based on the successful features of the one-dimensional model, a two dimensional formulation is also posed for the axisymmetric solution of a cylindrical waveguide. Although no results from the two dimensional formulation are presently available, the model could be used to analyze plasmas in configurations more representative of actual propulsion chambers. This would enable an examination of the thermal effects across the cross section and wall convective heat transfer.

5. REFERENCES

Asinovskii, E. I. and V. M. Batenin (1973). "High-Temperature State of a Plasma in a Powerful Microwave Discharge." High Temperature 11(2): 357-359.

Asmussen, J. (1989). "Electron cyclotron resonance microwave discharges for etching and thin-film deposition." Journal of Vacuum Science Technology A 7(3): 883-893.

Balaam, P. and M. M. Micci (1990). "The Stabilization and Spectroscopic Study of Microwave Generated Resonant Cavity Plasmas." AIAA/DGRL/JSASS 21st International Electric Propulsion Conference, Orlando, FL, AIAA-90-2635.

Batenin, V. M., A. A. Belevtsev, V. S. Zrodnikov, I. I. Klimovskii, V. I. Muranov and V. F. Chinov (1977). "Experimental Study of a Quasi-CW Discharge in Helium at High Pressures." Soviet Journal of Plasma Physics 3(6): 759-762.

Batenin, V. M., I. I. Klimovskii and V. R. Khamraev (1976b). "Propagation of a Microwave Discharge in Heavy Atomic Gases." Soviet Physics JETP 44(2): 316-321.

Batenin, V. M., V. S. Zrodnikov and V. F. Chinnov (1976a). "Microwave Discharge in Helium." High Temperature 14(1): 186-188.

Batenin, V. M., V. S. Zrodnikov, I. I. Klimovskii and N. I. Tsemko (1973). "Propagation Mechanism of an Ultrahigh-Frequency Discharge in Air." Soviet Physics JETP **36**(3): 449-452.

Batenin, V. M., V. S. Zrodnikov, V. K. Roddatis and V. F. Chinnov (1975). "Spectroscopic Investigation of a Microwave Discharge in Hydrogen." High Temperature **13**(2): 250-257.

Batenin, V. M., V. S. Zrodnikov, V. K. Roddatis and V. F. Chinnov (1976c). "Experimental Investigation of a Microwave Discharge in Helium." Soviet Journal of Plasma Physics **2**(5): 463-466.

Bethke, G. W. and A. D. Reuss (1969). "Microwave-Induced Plasma Shield Propagation in Rare Gases." The Physics of Fluids **12**(4): 822-835.

Beust, W. and W. L. Ford (1961). "Arcing in CW Transmitters." The Microwave Journal **4**(10): 91-95.

Deininger, W. D., A. Chopra and K. D. Goodfellow (1989). "Cathode Erosion Tests for 30 kW Arcjets." 25th AIAA/ASME/SAE/ASEE Joint Propulsion Conference, Monterey, CA, AIAA-89-2371.

Fuller, A. J. B. (1969). Microwaves. Exeter, Pergamon Press Ltd. Chpt. 4-5.

Golden, D. E. (1966). "Comparison of Low-Energy Total and Momentum-Transfer Scattering Cross Sections for Electrons on Helium and Argon." Physical Review **151**(1): 48-51.

Goorjian, P. M. (1990). "Algorithm Development for Maxwell's Equations for Computational Electromagnetism." 28th Aerospace Sciences Meeting, Reno, Nevada, AIAA-90-0251.

Hasegawa, M., A. Nishizawa, K. Sato and H. Ikezi (1975). "Filamentary Plasma Ignited by Microwaves in High Pressure Gases." Reports of Research Institute for Applied Mechanics 22(70): 155-164.

Hsu, W. L., D. M. Tung, E. A. Fuchs, K. F. McCarty, A. Joshi and R. Nimmagadda (1989). "Low-Temperature Diamond Growth in a Microwave Discharge." Applied Physics Letters 55(26): 2739-2741.

Jahn, R. G. (1968). Physics of Electric Propulsion. New York, McGraw-Hill Book Company. Chpt. 3-4.

Jeng, S. M. and D. R. Keefer (1987). "Numerical Investigation of Laser-Sustained Hydrogen Plasmas in a Forced Convective Flow." Journal of Propulsion and Power 3(3): 255-262.

Kapitza, P. L. (1969). "Free Plasma Filament in a High Frequency Field at High Pressure." Soviet Physics JETP 30(6): 973-1224.

Kapitza, P. L. and S. I. Filiminov (1972). "Apparatus for Production of a Free Plasma Filament. Determination of the Current and Resistance of the Filament." Soviet Physics JETP 34(3): 542-553.

Knecht, J. P. and M. M. Micci (1988). "Analysis of a Microwave-Heated Planar Propagating Hydrogen Plasma." AIAA Journal 26(2): 188-194.

Matsuzaki, R. (1982). "Analytical Expressions for Specific Heats and Isentropic Exponent of High Temperature Gases. I. Monatomic and Diatomic Gases." Japanese Journal of Applied Physics 21(7): 1003-1008.

Meierovich, B. E. (1972b). "Contribution of the Theory of an Equilibrium High-Frequency Gas Discharge." Soviet Physics JETP 34(5): 1006-1013.

Meierovich, B. E. (1973). "Diffusion in a High Frequency Gas Discharge." Soviet Physics JETP 36(2): 291-299.

Meierovich, B. E. and L. P. Pitaevskii (1972a). "On the Structure of the Transition Layer in a High-Frequency Gas Discharge." Soviet Physics JETP 34(1): 121-124.

Micci, M. M. (1984). "Prospects for Microwave Heated Propulsion." AIAA/SAE/ASME 20th Joint Propulsion Conference, Cincinnati, Ohio, AIAA-84-1390.

Miyake, S., S. Takeuchi and Y. Arata (1974). "Experimental Investigation of Coaxial Microwave Plasmatron in Nitrogen Gas." Japanese Journal of Applied Physics 13(2): 296-305.

Moore, C. E. (1949). Atomic Energy Levels. Washington D. C., U. S. Government Printing Office. pgs. 4-7.

Mueller, J. and M. Micci (1989). "Investigation of Propagation Mechanism and Stabilization of a Microwave Heated Plasma." AIAA/ASME/SAE/ASEE 25th Joint Propulsion Conference, Monterey, CA, AIAA-89-2377.

Mueller, J. and M. M. Micci (1988). "Numerical and Experimental Investigations of a Propagating Microwave-Heated Plasma." DGRL/AIAA/JSASS 20th International Electric Propulsion Conference, Garmisch-Partenkirchen, W. Germany, IEPC-88-100.

Mueller, J. and M. M. Micci (1990). "Microwave Electrothermal Thrusters Using Waveguide Heated Plasmas." AIAA/DGRL/JSASS 21st International Electric Propulsion Conference, Orlando, FL, AIAA-90-2562.

Mur, G. (1981). "Absorbing Boundary Conditions for the Finite-Difference Approximation of the Time Domain Electromagnetic-Field Equations." IEEE Transactions on Electromagnetic Compatibility **EMC-23**(4): 377-382.

Myshenkov, V. I. and Y. P. Raizer (1972). "Ionization Wave Propagating Because of Diffusion of Resonant Quanta and Maintained by Microwave Radiation." Soviet Physics JETP **34**(5): 1001-1005.

Offermanns, S. (1989). "Electrodeless High-Pressure Microwave Discharges." Journal of Applied Physics **67**(1): 115-123.

Owano, T. G., C. H. Kruger and R. A. Beddini (1991). "Electron-Ion Three Body Recombination Coefficient of Argon." AIAA 22nd Fluid Dynamics, Plasma Dynamics & Lasers Conference, Honolulu, Hawaii, AIAA-91-1488.

Pai, S.-i. (1962). Magnetogasdynamics and Plasma Dynamics. Englewood Cliffs, Prentice-Hall. Chpt. 2.

Raizer, Y. P. (1972). "Propagation of a High-Pressure Microwave Discharge." Soviet Physics JETP 34(1): 114-120.

Rhodes, R. and D. Keefer (1989). "Numerical Modeling of a Radio Frequency Plasma in Argon." AIAA Journal 27(12): 1779-1784.

Ridder, J. P. and R. A. Beddini (1989). "A Time Accurate Finite Volume Method for Propulsion Chamber Flows." AIAA/ASME/SAE/ASEE 25th Joint Propulsion Conference, Monterey, CA, AIAA-89-2554.

Sforza, P. F. (1969). "Nonlinear Interaction of a Microwave Field with a Plasma Slab in a Waveguide." Journal of Applied Physics 40(4): 1908-1917.

Tishchenko, E. A. and V. G. Zatsepin (1975). "Active Submillimeter Diagnostics of the Plasma of a Microwave Pinch Discharge at High Pressure." Soviet Physics JETP 41(2): 268-275.

Vargaftik, Ed. (1975). Tables on the Thermophysical Properties of Liquids and Gases. Washington, Hemisphere Publishing Corporation.

Venkateswaran, S., C. Merkle and M. Micci (1990). "Analytical Modelling of Microwave Absorption in a Flowing Gas." 21st Fluid Dynamics, Plasma Dynamics and Lasers Conference, Seattle, WA, AIAA-90-1611.

Weast, R. C., Ed. (1986). CRC Handbook of Chemistry and Physics. Boca Raton, CRC Press, Inc.

Whitehair, S. and J. Asmussen (1984). "Demonstration of a New Electrothermal Thruster Concept." Applied Physics Letters 44(10): 1014-1016.

Whitehair, S., L. L. Frasch and J. Asmussen (1987). "Experimental Performance of a Microwave Electrothermal Thruster with High Temperature Nozzle Materials." 19th AIAA/DGRL/JSASS International Electric Propulsion Conference, Colorado Springs, CO, AIAA-97-1016.

Yee, K. S. (1966). "Numerical Solution of Initial Boundary Value Problems Involving Maxwell's Equations in Isotropic Media." IEEE Transactions on Antennas and Propagation **AP-14**(3): 302-307.

APPENDIX: THERMODYNAMIC, TRANSPORT AND ELECTRODYNAMIC PROPERTIES

A.1 NOMENCLATURE

Property Table Variables:

C_+	ion concentration
f_{He}	electron partition function for the helium atom
f_{He^+}	electron partition function for the helium ion
h	Planck's constant
I_1	first ionization energy
K	Boltzman's constant
m_e	electron mass
n	number density of particles
n_e	number density of electrons
p	pressure
Q	collision cross section
q_e	electron charge
T	temperature
v_{th}	thermal velocity of particle collisions
ε	permittivity
ε_0	permittivity of free space
ν	collision frequency
σ	electrical conductivity
ω	angular microwave frequency
ω_p	angular plasma frequency

A.2 FORMULATION

The computation of the electromagnetic and fluid equation systems requires various property values of the fluid (gas) used. These values are found through a table look-up using a simple linear interpolation scheme. The table was developed such that all properties are indexed by pressure and temperature.

The values of c_p, c_v, γ, are found using the Saha relations. As such, the gas is assumed to be an equilibrium mixture of ideal gas species. For example, helium gas would be considered a mixture of He, He^+, and electrons, all at the same temperature. Let C_+ represent the concentration of helium ions in the mixture. Then using the Saha equation, the concentration of ions is given by

$$\frac{C_+^{\,2}}{(1-C_+)(1+C_+)} = \frac{2}{p}\left(\frac{2\pi m_e}{h^2}\right)^{1.5} (KT)^{2.5} \left(\frac{f_{He^+}}{f_{He}}\right) \exp\left(-\frac{I_1}{KT}\right) \qquad \text{(A1)}$$

where all units are in mks. The electron partition functions for the ion and neutral atom have the basic form

$$f = g_0 + g_1 \exp\left(\frac{h' c w_1}{KT}\right) \qquad \text{(A2)}$$

where the values for g_0, g_1, and w_1 (cm^{-1}) were taken from Atomic Energy Levels by C.E. Moore (1949). The properties, c_p, c_v, γ, and the density, ρ, are then calculated using perfect gas relations (Matsuzaki, 1982).

The values for viscosity and thermal conductivity were taken from Tables on the Thermophysical Properties of Liquids and Gases (Vargaftik, 1975) and the CRC Handbook of Chemistry and Physics (Weast, 1986) respectively. This data does not include the entire temperature range needed, so a linear extrapolation of the data was done. Also, it was assumed that there is no pressure dependence for the range used.

Since the permittivity and electrical conductivity of the gas depend on the microwave frequency, the values of the plasma frequency squared, ω_p^2, and the effective collision frequency, ν, are stored in the table. The values of the permittivity and conductivity are then found within the program by the formulae

$$\sigma = \frac{\varepsilon_0 \nu \omega_p^2}{\omega^2 + \nu^2} \tag{A3}$$

and

$$\varepsilon = \varepsilon_0 \left(1 - \frac{\omega_p^2}{\omega^2 + \nu^2}\right) \tag{A4}$$

where ω is the angular frequency of the input microwave. The plasma frequency squared is given by

$$\omega_p^2 = \frac{n_e q_e^2}{\varepsilon_0 m_e} \tag{A5}$$

where n_e is the number density of electrons, q_e is the charge of an electron, ε_0 is the permittivity of free space, and m_e is the mass of an electron. The effective collision frequency is given by

$$\nu = \nu_{ei} + \nu_{en} \tag{A6}$$

where ν_{ei} represents the electron-ion collision frequency and ν_{en} represents the electron-neutral atom collision frequency. In each case, the collision frequency may be expressed as

$$\nu = n Q v_{th} \tag{A7}$$

where Q is the cross sectional area for the collision and v_{th} is the thermal velocity which is assumed to be a Boltzman distribution and is thus given by

$$v_{th} = \sqrt{\frac{8KT}{\pi m_e}}. \tag{A8}$$

The cross section for electron-ion collisions, the coulomb cross section, can be accurately calculated theoretically (Jahn, 1968).

$$Q_{ei} = \frac{\pi q_e^4}{(4\pi\varepsilon_0)^2\left(\frac{3}{2}KT\right)^2} \ln\left[\frac{8\pi\varepsilon_0\left(\frac{3}{2}KT\right)}{q_e^2}\sqrt{\frac{\varepsilon_0 KT}{n_e q_e^2}}\right] \tag{A9}$$

The cross section for electron-neutral collisions, however, is based on an empirically derived formula taken from the work by D. E. Golden (1966). The value used in the program is twice that of the cross section found in the referenced work. This was done to achieve closer pressure dependence of the properties as shown in the works of Batenin, et al. (1977) and Mueller and Micci (1989). Following are some plots of the resulting property values derived from the tables.

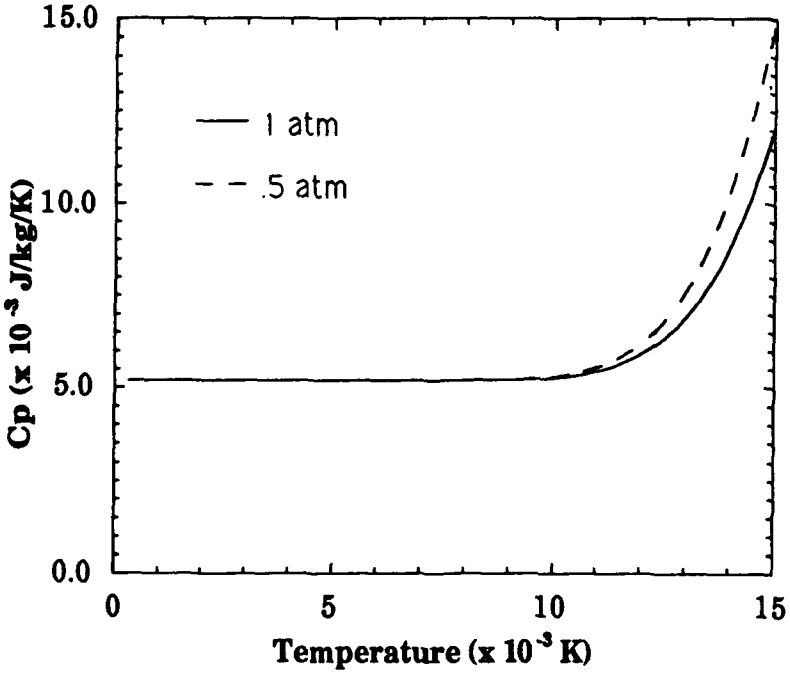

Figure A1. Specific heat values for helium at .5 and 1 atmosphere pressure.

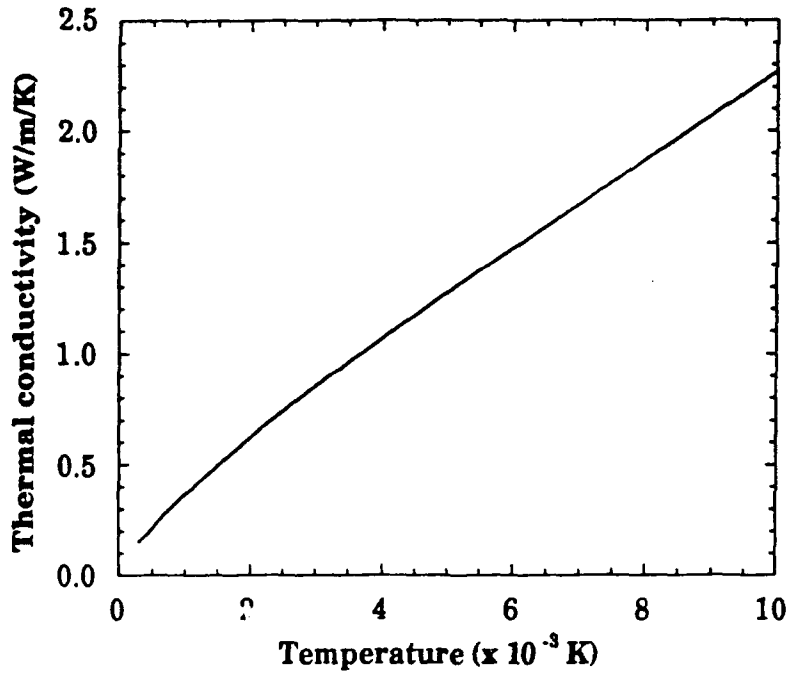

Figure A2. Thermal conductivity of helium.

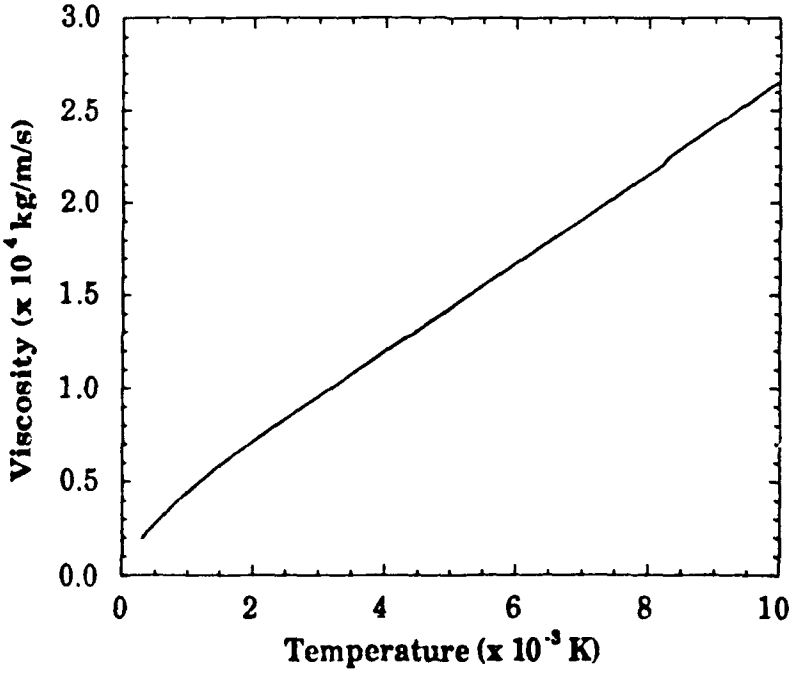

Figure A3. Viscosity values for helium.

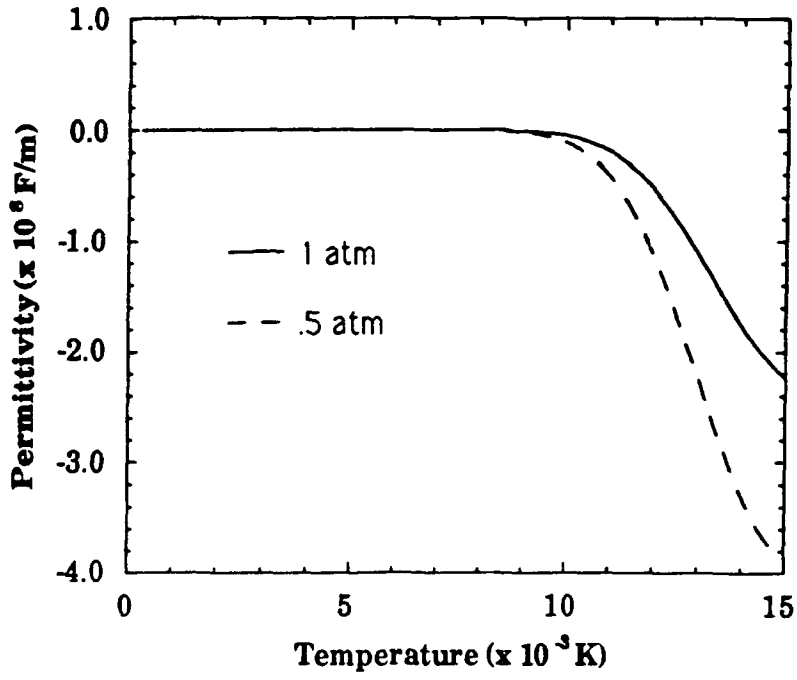

Figure A4. Permittivity values for helium at .5 and 1 atmosphere pressure

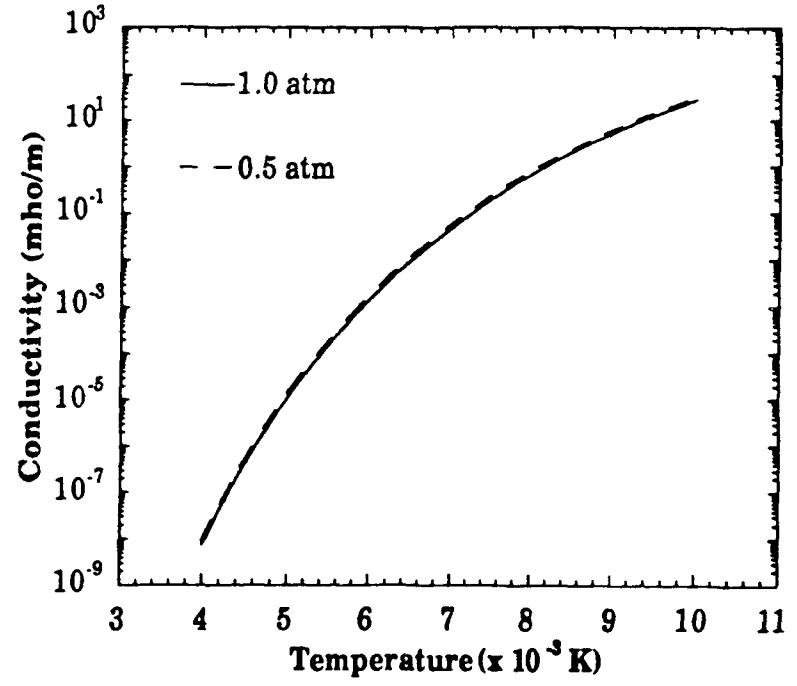

Figure A5. Electrical conductivity values for helium at .5 and 1 atmosphere pressure.

APPENDIX B: STUDENTS SUPPORTED

During the period of this grant, principal support was provided to the following student:

Mark J. Mueller, MS in Aeronautical and Astronautical Engineering, August, 1991.

Partial support for one semester was also provided to:

Anne Audibert, MS in Aeronautical and Astronautical Engineering, May, 1991.

APPENDIX C: PUBLICATIONS

The following publications have resulted from this grant:

1) Owano, T.G., Kruger, C.H. and Beddini, R.A.: *Electron-Ion Three Body Recombination Coefficient of Argon,* AIAA paper no. 91-1488, AIAA 22nd Fluid Dynamics, Plasma Dynamics and Lasers Conference, June 1991.

2) Mueller, M. J. and Beddini, R.A.: *Nonsteady Propagation of a Microwave Plasma in a Waveguide*, anticipated, based on material in this report, 1992.